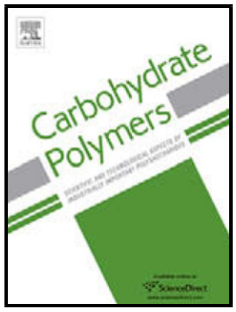

Title: On the formation of Bi_2S_3-cellulose nanocomposite films from bismuth xanthates and trimethylsilyl-cellulose

Authors: David Reishofer, Heike M. Ehmann, Heinz Amenitsch, Christian Gspan, Roland Fischer, Harald Plank, Gregor Trimmel, Stefan Spirk

PII: S0144-8617(17)30128-5
DOI: http://dx.doi.org/doi:10.1016/j.carbpol.2017.02.008
Reference: CARP 11987

To appear in:

Received date: 5-10-2016
Revised date: 1-2-2017
Accepted date: 2-2-2017

Please cite this article as: Reishofer, David., Ehmann, Heike M., Amenitsch, Heinz., Gspan, Christian., Fischer, Roland., Plank, Harald., Trimmel, Gregor., & Spirk, Stefan., On the formation of Bi2S3-cellulose nanocomposite films from bismuth xanthates and trimethylsilyl-cellulose.*Carbohydrate Polymers* http://dx.doi.org/10.1016/j.carbpol.2017.02.008

On the formation of Bi_2S_3-cellulose nanocomposite films from bismuth xanthates and trimethylsilyl-cellulose

David Reishofer[1,4], Heike M. Ehmann[1], Heinz Amenitsch[2], Christian Gspan[3], Roland Fischer[2], Harald Plank[3], Gregor Trimmel[1], Stefan Spirk[1,4,5*]

[1]*Institute for Chemistry and Technology of Materials, NAWI Graz, Graz University of Technology, Stremayrgasse 9, 8010 Graz, Austria.*

[2]*Institute for Inorganic Chemistry, Graz University of Technology, Stremayrgasse 9, 8010 Graz, Austria.*

[3]*Graz Centre for Electron Microscopy, Steyrergasse 17, A-8010 Graz, Austria*

[4]*Institute for the Engineering and Design of Materials, University of Maribor, Smetanova 17, 2000 Maribor, Slovenia.*

[5]*Institute for Paper, Pulp and Fiber Technology, Inffeldgasse 23(A), 8010 Graz, Austria*

Members of the European Polysaccharide Network of Excellence (EPNOE).

To whom correspondence should be addressed: stefan.spirk@tugraz.at

Highlights:

Cellulose-Bi_2S_3 nanocomposites have been prepared.

The formation of the nanoparticles was investigated using in-situ GISWAXS.

The properties of the nanocomposite have been investigated in detail.

Abstract

The synthesis and characterization of bismuth sulfide-cellulose nanocomposite thin films was explored. The films were prepared using organosoluble precursors, namely bismuth xanthates for Bi_2S_3 and trimethylsilyl cellulose (TMSC) for cellulose. Solutions of these precursors were spin coated onto solid substrates yielding homogeneous precursor films. Afterwards, a heating step under inert atmosphere led to the formation of thin nanocomposite films of bismuth sulfide nanoparticles within the TMSC matrix. In a second step, the silyl groups were cleaved off by vapors of HCl yielding bismuth sulfide/cellulose nanocomposite films. The thin films were characterized by a wide range of surface sensitive techniques such as atomic force microscopy, attenuated total reflection infrared spectroscopy, transmission electron microscopy and wettability investigations. In addition, the formation of the nanoparticle directly in the TMSC matrix was investigated *in situ* by GI-SWAXS using a temperature controlled sample stage.

Keywords: cellulose nanocomposite, trimethylsilyl cellulose, ATR-IR, GI-SWAXS, bismuth sulfide

1. Introduction

In recent years, research on semiconducting colloidal crystals led to a wide range of solution-processable optoelectronic devices such as photocatalysts, light emitting devices, sensors, and photovoltaic cells. However, many of the used materials contain toxic metals such as cadmium or lead having a negative impact on the environment during manufacturing and after disposal. A sulfide forming element with a rather low reported toxicity is bismuth. Bi_2S_3 nanoparticles and nanocomposites find numerous applications in magnetic resonance imaging (Rabin, Manuel Perez, Grimm, Wojtkiewicz, & Weissleder, 2006), thermoelectric devices (Y. Y. Wang, Cai, & Yao, 2012), memory devices (Liu et al., 2013), photodetectors (Konstantatos, Levina, Tang, & Sargent, 2008), as electrode material in lithium-ion batteries (Jung, Park, & Sohn, 2011), as well as in electronic, optoelectronic and gas sensor devices (Ahmad, Rafiq, Rasool, Imran, & Hasan, 2013; Li, Yang, Zhang, & Zhou, 2012; Yao et al., 2008; Yao et al., 2006). In optoelectronic devices, the low band gap of bismuth sulfide (1.3 to 1.7 eV (Liu et al., 2013)) is exploited for instance. (Martinez et al., 2013; Z. Wang et al., 2010). A very convenient route to produce bismuth sulfide nanoparticles in synthetic polymer matrices is to use soluble bismuth xanthate (BiXa) precursors which are decomposed after the final processing step e.g., spin coating or knife blading (Kaltenhauser et al., 2013). In that case, a functioning solar cell was assembled using this nanocomposite thin film as a functional layer. These works inspired us to explore whether polysaccharide derivatives could be implemented in such layers. It can be expected that they are capable to act as stabilizing agents to control the growth of the Bi_2S_3 nanoparticles generated from xanthate precursors to obtain nanocomposites with a better ecological footprint. The major challenge to obtain homogeneous nanocomposites is to find a common solvent for both, the BiXa precursor and the polysaccharide derivative. Since many bismuth xanthates are readily soluble in apolar organic solvents, trimethylsilyl cellulose (TMSC) was chosen as polysaccharide due to its

excellent solubility in aprotic solvents at high degrees of substitution with TMS groups. TMSC has several further advantages in this context: its solubility can be fine-tuned by the degree of substitution, it is rather light- and thermostable under exclusion of air/moisture (Wolfberger et al., 2015) and it is a good film forming polymer (T. Mohan et al., 2013; Orelma, Filpponen, Johansson, Laine, & Rojas, 2011). Further, the conversion into cellulose proceeds via a gas phase reaction employing vaporous HCl (Ehmann et al., 2015; Eero Kontturi & Lankinen, 2010). In contrast to other regeneration procedures, the nanocomposite films do not come in contact with any liquids during the regeneration, preventing undesired alterations in terms of morphology and structure. The regeneration procedure using acidic vapors was just recently exploited to generate metallic Bi-NP/cellulose nanocomposites in a very efficient way by photoreduction of a bismuth precursor in toluene solution (Breitwieser et al., 2015). An advantage by using biobased materials in such nanocomposites is to circumvent or at least reduce the use of synthetic polymers in advanced materials to lower the impact on the environment. Particularly cellulosic materials are well suited for this purpose since they are renewable and, if the degree of substitution with functional groups is low, they are also biodegradable. In the case of TMSC, it was already demonstrated some decades ago that this particular cellulose derivative has a rather good life cycle performance.(Cooper, Sandberg, & Hinck, 1981)

Here, we combine the TMSC precursor route for cellulosic thin films with the BiXa strategy to generate Bi_2S_3 nanoparticles. The goal is to realize Bi_2S_3 cellulose nanocomposite thin films. The particular role of the TMSC is to provide a matrix which allows for controlling the growth and shape of the nanoparticles.

The paper is constructed as follows: after a detailed characterization of the film forming properties of various BiXa/TMSC films, these films were thoroughly analyzed and subjected to a

heat treatment. The formation of the particles was monitored by *in-situ* grazing incidence X-ray scattering using a temperature controlled heating stage. All samples have been analyzed in detail after the heating step and after conversion to cellulose using HCl vapors was accomplished.

2. Experimental

2.1 Materials

Trimethylsilyl-cellulose (TMSC; Avicel pulp DS: 2.7-2.9), purchased from TITK Rudolstadt, and bismuth xanthate (bismuth(III)-O-3,3-dimethylbutan-2-yl dithiocarbonate, denoted as BiXa in the following), synthesized according to a literature procedure, (Kaltenhauser et al., 2013) were used as starting materials for the thin film preparation. Hydrochloric acid (37 wt.%), chloroform (99 wt.%) and sulfuric acid (95 wt.%) were purchased from VWR chemicals. Hydrogen peroxide (30 wt.%) was obtained from Sigma-Aldrich. All chemicals were used without further purification. Silicon wafers (Siegert Wafer), glass slides (Roth), Au-coated glass slides (SPR102-AU), Filter Chromafil® Xtra PVDF-45/25 0.45 µm, petri dishes (20 ml; 5 cm diameter) were used as obtained.

2.2. Methods

2.2.1 ATR-IR spectroscopy

The experiments were performed with an ALPHA FT-IR spectrometer (Bruker; Billerica, MA, USA). For the measurements, an attenuated total reflection (ATR) unit was used with 48 scans at a resolution of 4 cm^{-1} and a scan range between 4000 and 400 cm^{-1}. The data was analyzed with OPUS 4.0 software.

2.2.2. AFM

Atomic force microscopy (AFM) images were recorded in the tapping mode (non-contact mode) on a Veeco Multimode Quadrax MM AFM (Bruker; Billerica, MA, USA). For the scanning, silicon cantilevers (NCH-VS1-W from NanoWorld AG, Neuchatel, Switzerland) were used with an average spring constant of 42 N/m (Force Constant) and with a resonance frequency of 270 – 320 kHz. All measurements were performed at room temperature and under ambient atmosphere. The calculation of the root mean square roughness (calculated from a 6 x 6 µm image) and the image processing was done with the Nanoscope software (V7.30r1sr3; Veeco).

2.2.3. Stylus profilometry/Determination Film Thickness

Layer thickness was measured on a Bruker DekTak XT surface profiler. The scan length was set to 1000 µm over the time duration of 3 seconds. The diamond stylus had a radius of 12.5 µm and the force was 3 mg with a resolution of 0.333 µm/sample and a measurement range of 6.5 µm. The profile was set to *hills and valleys*. For the determination of the film thickness a silicon wafer sample was scratched five times (up to the silicon surface). This measured profile was then used to calculate the thickness of the different coatings.

2.2.4 Contact angle and surface free energy determinations

To determine the static contact angle and the surface free energy (SFE), a drop shape analysis system DSA100 (Krüss GmbH, Hamburg, Germany) with a T1E CCD video camera (25 fps) and the DSA1 v 1.90 software was used. For the measurements, 3 µl droplets of Milli-Q water (≥18 $M\Omega\ cm^{-1}$) and diiodomethane as test liquids in the sessile drop mode were deposited on the substrates at 25 °C. Each sample was measured at least three times. The contact angle

calculations were performed using the Young-Laplace equation and for the determination of the surface free energy the Owens-Wendt-Rabel & Kaelble method was employed.

2.2.5. UV-Vis spectroscopy

The UV-Vis absorption spectra of the samples (on glass substrate) were measured on a Shimadzu UV-1800 UV spectrophotometer. The absorbance was determined in a range from 200 - 1100 nm at 25 °C under ambient atmosphere.

2.2.6. GI-SWAXS

The 2D *in situ* GISAXS and GIWAXS experiments were performed at the high-flux SAXS beamline 5.2L of the electron storage ring ELETTRA (Trieste, Italy). The X-ray energy was 8 keV. The beamline has been adjusted to a q-resolution ($q=4\pi/\lambda*\sin(2\theta/2)$, 2θ being the scattering angle) between 0.1 and 3.5 nm^{-1} (GISAXS). During the temperature scan, data were recorded with framing rate of 6 s using a Pilatus 1M detector (Dectris). For detection of the GIWAXS signal, a Pilatus 100K detector from Dectris was used. As calibration standard silver behenate with a lamellar spacing of 58.38 Å and p-bromo benzoic acid were used. The sample-to-detector distance was 1516.55 mm and the incidence angle was set to 0.83°.

The *in situ* heating was performed using the Anton Paar DHS1100 heating stage (temperature range 5-1100 °C, sealed with Kapton windows) which was continuously rinsed with gaseous nitrogen under steady flow conditions. The heating rate was set to 10 °C/min.

2.2.7. Scanning Transmission Electron Microscopy (STEM)

STEM investigations were done on a Titan³ G2 60-300 from FEI at 300 keV accelerating voltage. The microscope is equipped with a CS-corrector to correct the spherical aberration in the STEM

mode to obtain atomic high resolution with a lateral resolution below 1 Ångström. Bright field (BF) and high angle annular dark field (HAADF) STEM images were recorded with detectors from Gatan. Energy dispersive X-ray spectroscopy (EDXS) was performed with four high-sensitivity SDD X-ray spectrometers (Super-X) from Bruker. The STEM image was further used for the determination of the nanoparticle size distribution.

2.2.8. Film Preparation

The different substrates (silicon wafers (1.4 x 1.4 cm), glass slides (1.4 x 1.4 cm) and gold coated glass slides (2.0 x 1.0 cm)) were cleaned with "piranha" acid (H_2SO_4:H_2O_2 = 7:3 (v/v)) for 30 min (10 min for gold slides) and neutralized afterwards with distilled water. For the film preparation, TMSC (1 wt.%) was dissolved in $CHCl_3$, filtered and combined (1:1 (v/v)) with the bismuth xanthate solution (1 wt.%, 5 wt.%, 10 wt.% in $CHCl_3$). The solution (180 µl) was deposited onto the different substrates and spin coated at 4000 rpm for 60 s (acceleration 2500 rpm/s). The *in-situ* synthesis of the Bi_2S_3 nanoparticles was performed by thermal conversion (185 °C over a period of 30 min, heating rate = 10 °C/min) of bismuth xanthate on a heating plate. After the thermal conversion, the films were exposed to HCl vapors for 12 minutes (created by 2 ml 12 wt% HCl in a petri dish) to obtain fully regenerated cellulose/Bi_2S_3-nanoparticle thin films.

3. Results and Discussion

3.1. Film preparation

The first step in the preparation of the nanocomposite thin films was to evaluate under which conditions homogenous films of TMSC and BiXa were formed by spin coating (Figure 1). We

chose as starting point 1 wt.% solutions of TMSC in $CHCl_3$ and added different amounts of BiXa (1, 5, and 10 wt.% in $CHCl_3$, respectively).

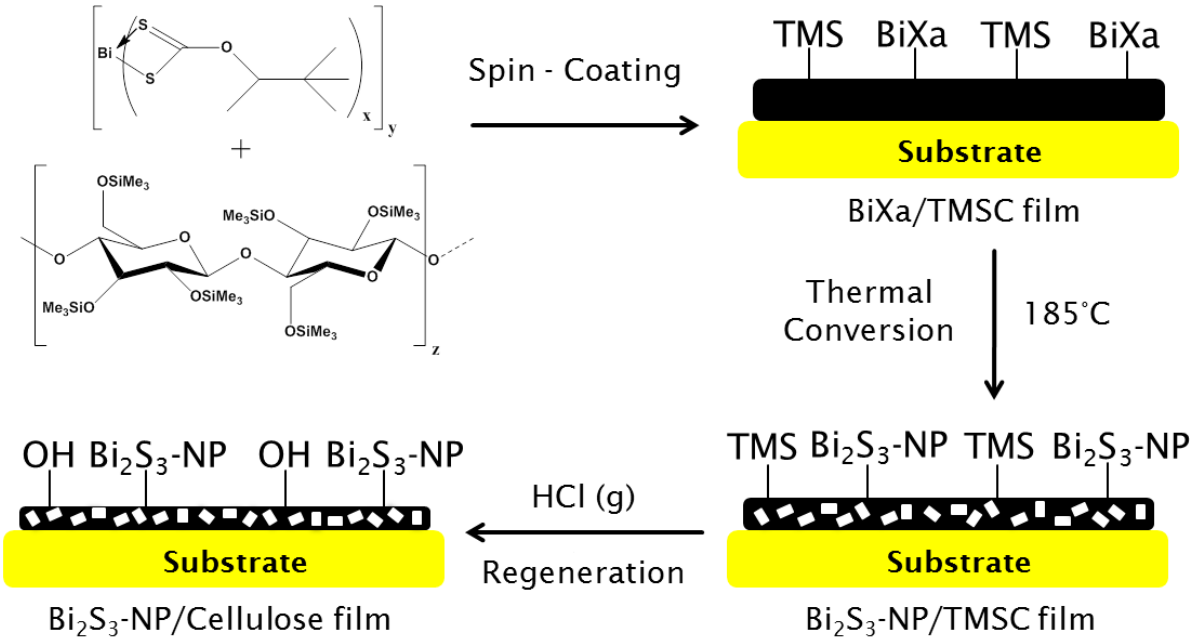

Figure 1. Schematic representation of the manufacturing steps of BiXa/TMSC nanocomposite films.

In all cases, macroscopically clear solutions were obtained which were stable over a period of more than 30 minutes. These solutions were placed on silicon substrates and subjected to spin coating (4000 rpm, 2500 rpm s, t = 60 s). After spin coating, all the films showed a smooth and homogeneous appearance by naked eye, which already gave a first hint that TMSC and BiXa were compatible in both, solution and solid state. The next step was to evaluate the thermal conversion of the BiXa to the Bi_2S_3 particles inside the films. It is known from literature (Kaltenhauser et al., 2013) that BiXa starts to decompose at ca 150 °C to form Bi_2S_3 concomitant with the formation of other volatile compounds. COS and 3,3-dimethylbut-1-ene are the typical species of the decomposition of xanthates via the Chugaev rearrangement (Pradhan, Katz, &

Efrima, 2003). Although H_2S is not directly formed via the Chugaev mechanism, traces may evolve during the decomposition of BiXa via other pathways. This could potentially lead to (partial) regeneration of TMSC via acid induced desilylation to cellulose along with the release of TMSCl as reported for related cases where HCl vapors have been employed. (Eero Kontturi, Thüne, & Niemantsverdriet, 2003)

3.2. ATR-IR spectroscopy

A very suitable method to monitor chemical reactions such as hydrolysis in thin films is ATR-IR spectroscopy. It can be clearly seen in Figure 2 (A) that neither the addition of the xanthate to the TMSC, nor the heating step caused regeneration of TMSC to cellulose.

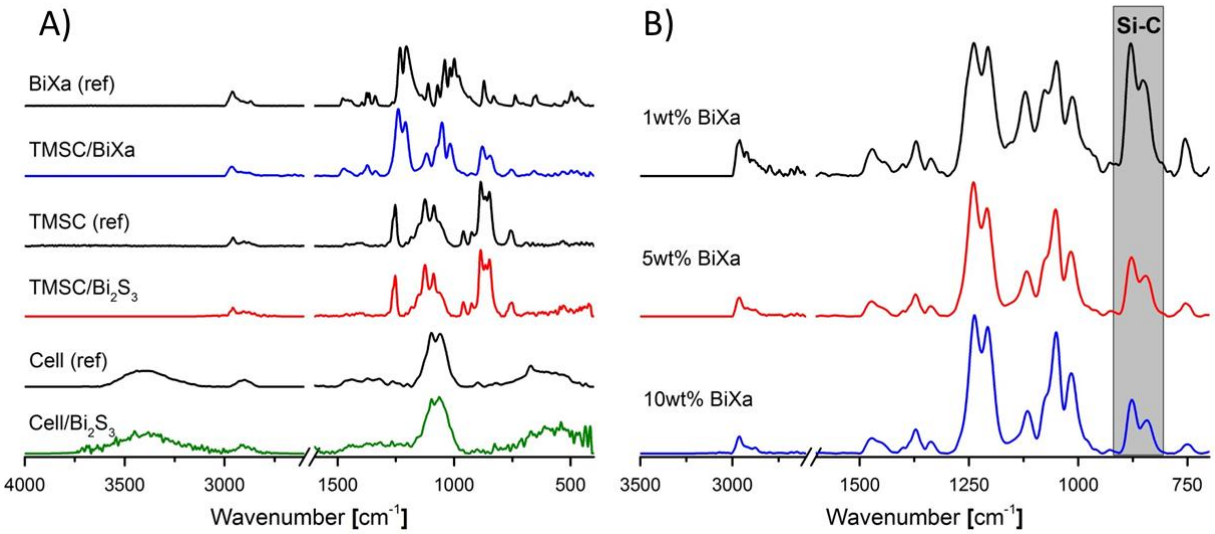

Figure 2. A) Comparison of the ATR IR reference spectra (BiXa, TMSC and cellulose) with nanocomposite thin films having a BiXa concentration of 5 wt.%. B) Comparison of ATR IR spectra of TMSC/BiXa nanocomposites at different BiXa contents. More data is available in the Supplementary Materials (Fig. S1 and S2)

For the non-treated BiXa/TMSC film, typical bands for xanthates as well as for TMSC were detected. The bands at 1238 cm^{-1} and 1207 cm^{-1} can be attributed to the asymmetric C–O–C stretching vibrations, and those at 1047 and 1017 cm^{-1} to the C–S stretching vibrations of the xanthate.

For the TMSC fraction, the Si-C vibration at 852 cm^{-1} and 752 cm^{-1} are characteristic. By increasing the amount of BiXa in the films, the relative intensity of bands associated with TMSC was significantly reduced (Fig 2B) since the spectra have been normalized on TMSC band at 1462 cm^{-1}. Therefore any incorporation of compounds into the film, will decerase the relative intensity of bands solely corresponding to TMSC. For instance, the band at 1121 cm^{-1} can be assigned to symmetric C–O–C stretching vibrations of both, TMSC and BiXa; therefore the relative band intensities remained rather constant by increasing the BiXa content. Bands associated with the BiXa (1238 cm^{-1}, 1207 cm^{-1}) vanished after exposure to elevated temperatures indicating a decomposition of the xanthate, while leaving the TMSC untouched. This was proven by a distinctive spectrum for TMSC exhibiting all characteristic bands for Si-C and Si-O-C vibrations. It can be concluded that neither the heating step at 195 °C nor the formed volatile side products in the conversion of BiXa to Bi_2S_3 caused the TMSC films to regenerate. However, a separate HCl treatment indeed induced regeneration from TMSC to cellulose as proven by the appearance of typical bands associated with cellulose at 1024 cm^{-1} (C–O stretching; aromatic C–H in plane deformation), 1064 cm^{-1} (C–O stretching) and 3000–3600 cm^{-1} (OH stretching) (T. Mohan et al., 2012).

3.3. Particle formation - GI-SWAXS and STEM

In order to get more insights in the heat-induced conversion of the BiXa into the corresponding bismuth sulfides, combined GI-SAXS and GIWAXS studies using monochromatic X-rays have

been performed. The setup of the experiment comprised a temperature-controlled sample stage which was flushed with dry nitrogen to prevent oxidation by air during the illumination with the synchrotron beam. After positioning the samples, the temperature was steadily increased and the scattering patterns were recorded. It can be clearly seen that the scattering contrast started to increase at ca 120 °C and reaches a maximum at ca. 195 °C. This can be attributed to the formation of Bi_2S_3 nanoparticles, which provide a higher scattering contrast compared to the small precursor molecules (Fig. 3) The formation of the nanoparticles was further evidenced in two movies demonstrating the heat induced conversion of BiXa to Bi_2S_3 (Supplementary materials section). Further proof for the presence of the bismuth sulfides was provided by analysis of the reflection planes of the GI-WAXS patterns (Fig. 4). The main diffraction peaks at 2.8 Å, 3.1 Å, 3.5 Å, 3.7 Å, 3.9 Å, 5.4 and 7.0 Å were nearly identical as those reported for orthorhombic Bi_2S_3 in literature (Joint Committee on Powder Diffraction Standards JCPDS Card No. 17-320).

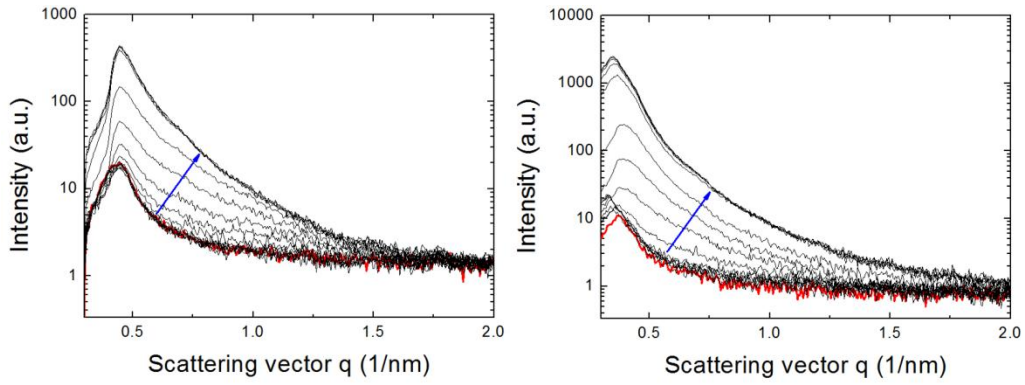

Figure 3. Heat induced growth of Bi_2S_3 nanoparticles in a TMSC film upon increase of temperature from 25 to 195 °C monitored by *in situ* GI-SAXS. Left: TMSC:BiXa ratio of 1:1, Right: TMSC: BiXa ratio of 1:10. Please note the different intensity scales for both scattering curves.

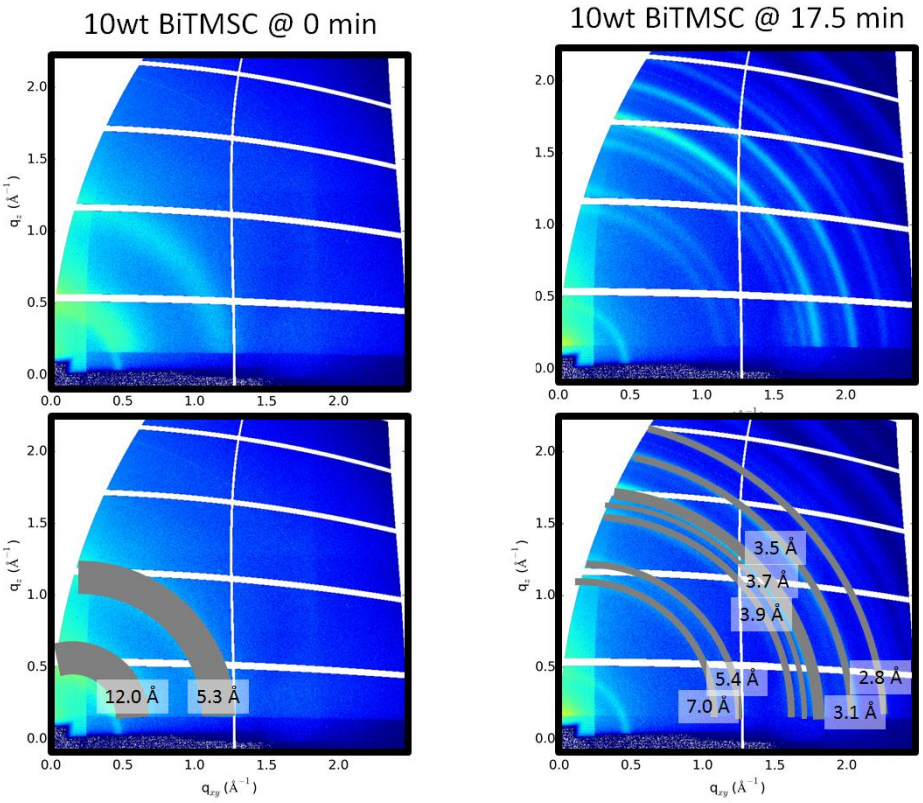

Figure 4. Scattering patterns of a TMSC/BiXa film before and after the heating procedure monitored by *in situ* GI-WAXS. The BiXa concentration was 10 wt.% in those films.

A crucial question is the shape and the size of the nanoparticles grown in the film. Besides SWAXS, bright field and high angle annular dark field TEM are very suitable methods to determine particle dimensions in thin films. However, sample preparation was a bit tricky, since we had to ensure the same conditions for the TEM sample as for the other films using Si-wafers as support. Since the films could not be peeled off the substrate nor deposited onto carbon grids (the polymer coating melts at 150 °C) we decided to deposit the TMSC/BiXa mixture on a NaCl grid, followed by the heating step and subsequent careful dissolution of the grid in water. Figure 5 illustrates the results of the 5 wt.% BiXa sample with different magnifications after the heating

step. The images indicated that the formed nanoparticles were rod shaped with a diameter of 25±4 nm and a length of 80±7 nm. An EDX spectrum of the Bi_2S_3 nanoparticles is depicted in the supporting materials (Fig. S4). Most of the particles were homogenously distributed in the matrix. However, some spots feature a higher particle density. The origins of this behavior remain unclear and could be either related to sample preparation or to the particle growth (Figure 5).

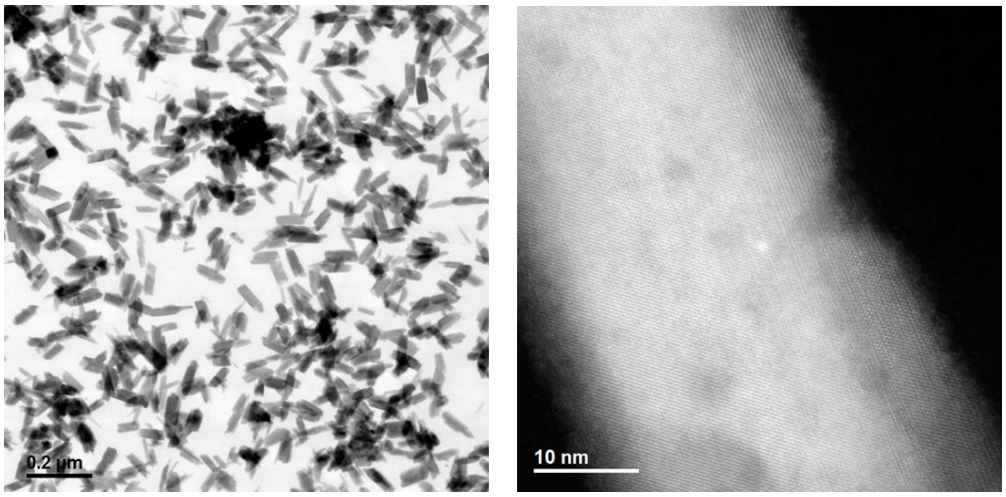

Figure 5. Bright field (left) and high angle annular dark field (right) TEM images of 5 wt.% Bi_2S_3-NP in a TMSC matrix at different magnifications.

3.4. Morphology - AFM

While the above mentioned methods clearly provided proofs for the successful conversion of the BiXa to the sulfides, a very interesting question was to which extent the morphology was affected by the heating process. It can be clearly seen that the heating process itself did not induce changes in neat TMSC. However, the addition of BiXa into the TMSC matrix led to slightly rougher surfaces. Interestingly, the effect of the concentration on morphology on non-treated

films was rather small (Table S2; Supplementary materials). However, situation changed after the heat treatment. All the images showed homogenously distributed features and a significant increase in the roughness of the films, relating to the amount of BiXa in the films.

The morphology of the nanocomposite films was analyzed by atomic force microscopy before and after the modification steps. In Figure 6, the AFM images of the non-treated films (A, D, G, J) at three different xanthate concentrations and there modifications (B, C, E, F, H, I, K, L) are depicted. The images clearly showed that particles were formed.

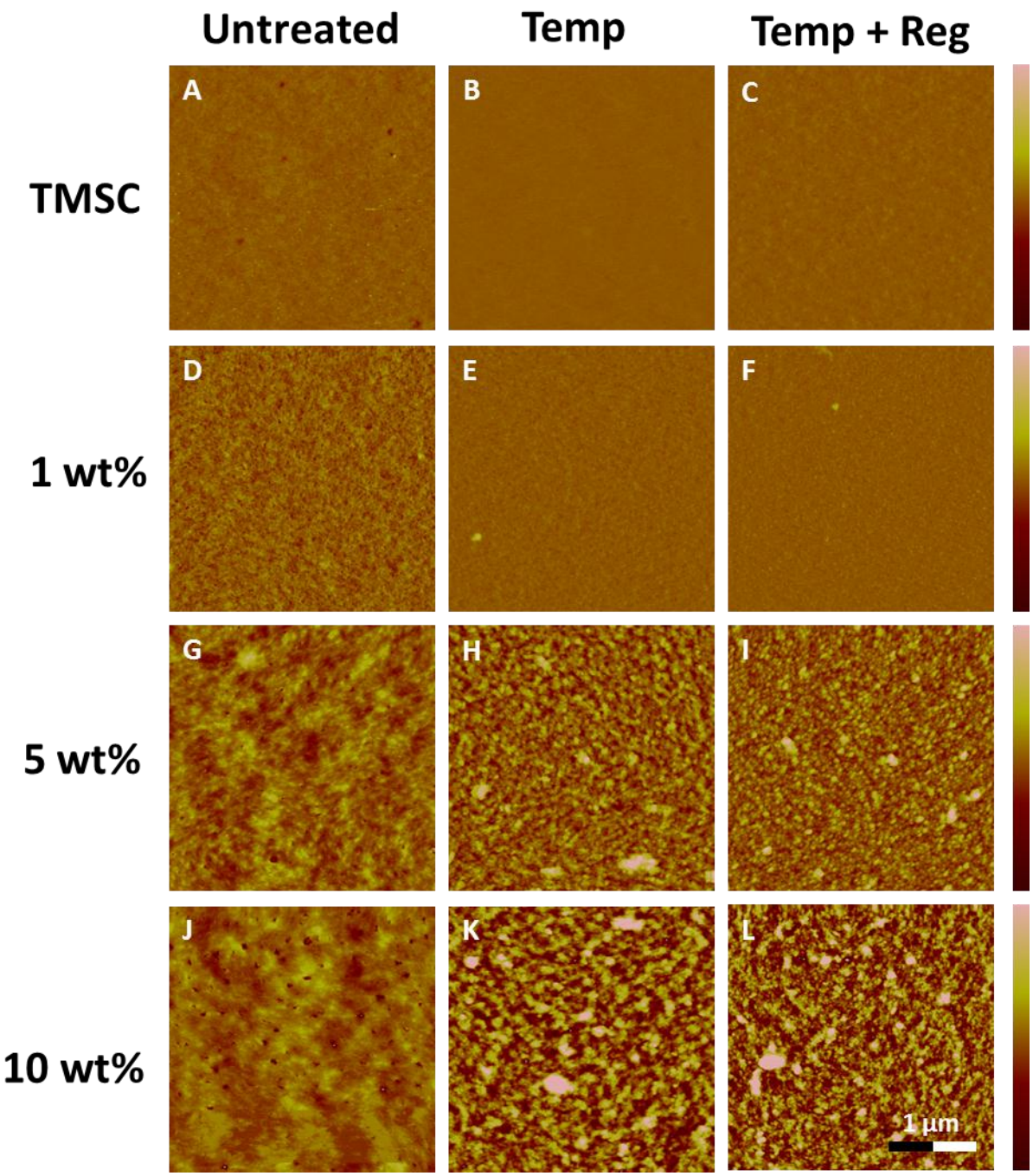

Figure 6. TMSC matrix (A, B, C) with 1 wt.% BiXa (D, E, F), 5 wt.% BiXa (G, H, I), 10 wt.% BiXa (J, K, L); Z-scale (A, D, G, J) = 40 nm, Z-scale (B, C, E, F, H, I, K, L) = 130 nm

The surface morphology as well as the roughness of the native films was altered by increasing the BiXa concentration (see Table S2). However, after the heating step, 80-100 nm small structures

are present in the films which can be attributed to the generated Bi_2S_3 nanoparticles. For the films containing 5 and 10 wt.% BiXa, this effect was very pronounced (Figure 6, H and K) while the surface morphology of the film containing 1 wt.% BiXa was not affected (for a smaller Z-scale see Fig. S5, Supplementary aterials). Besides changes in morphology, the film thickness decreased since a large fraction (67 wt.%) of BiXa consists of organic material, which was converted to volatile compounds during the heating step, finally leaving the TMSC film. Consequently, the decrease in layer thickness correlated with the amount of BiXa in the films. The 1 wt.% samples featured a decrease of 103 to 62 nm, the 5 wt.% from 248 to 92 nm and the largest decrease was observed for the 10 wt.% sample (482 to 118 nm). As films shrank, the roughness of the surface increased, especially for the samples containing 5 wt.% (2.83 nm to 11.4 nm) and 10 wt.% (2.78 nm to 20.9 nm) BiXa.

After the heat treatment step, the TMSC fraction of the nanocomposite was converted to cellulose by exposing the films to vaporous HCl over a period of 12 minutes. Although the thickness of the films decreased again after the regeneration of the material due to the loss of silyl groups, the morphology as well as the roughness remained unaffected by the treatment. During the entire modification process (heating and regeneration) the film thickness was reduced by 75 – 80% of their initial values.

3.5. Surface wettability and surface free energy

A further aspect when it comes to applications is the wettability of the nanocomposites and their interaction with other materials. Particularly the surface free energy (SFE) is an important parameter in the design of multi-layer applications. Therefore, the contact angles of different liquids (water and diiodomethane, Fig. S6, Supplementary materials) of the nanocomposites were determined using the sessile drop approach.

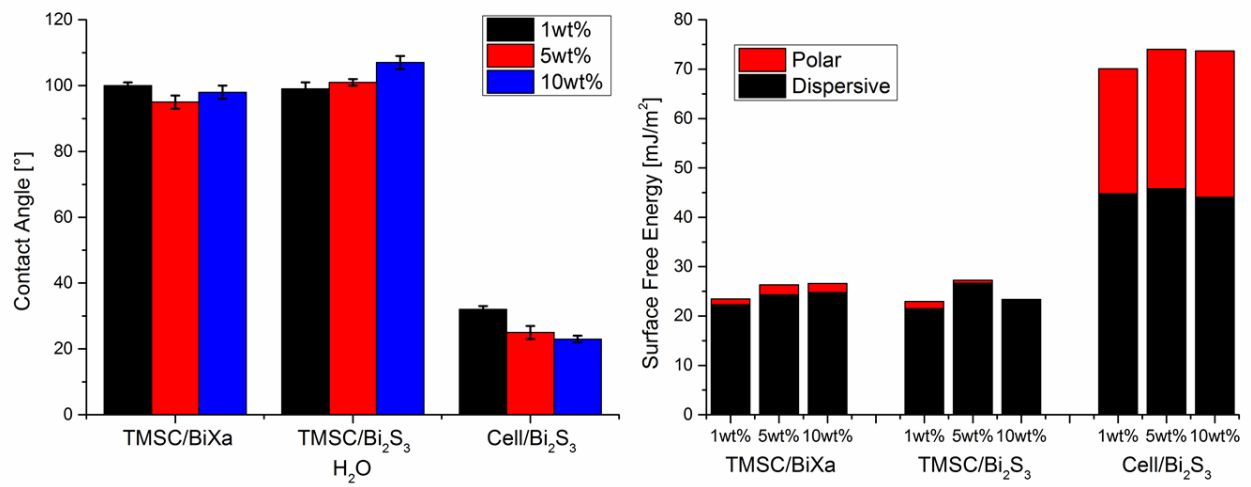

Figure 7. Static water contact angles and surface free energies of the native, heat treated and regenerated sample.

As shown in Figure 7, the non-treated TMSC/BiXa films exhibited static water contact angles of ca 100°, regardless of the BiXa concentration used for film preparation. Interestingly, even after the heat treatment step, i.e. the conversion of BiXa to Bi_2S_3, the films retained their hydrophobic character with just minor differences compared to the non-treated ones. These minor differences may be related to alterations in surface roughness, although we do not have hard evidence for this. Moreover, this data was a further proof (besides IR spectroscopy) that the TMS groups were not cleaved off by the formed volatile side products during BiXa decomposition. This was

reflected in the SFE of those films featuring a rather large dispersive and a low polar contribution. After a final HCl treatment step, the water contact angles decreased to values which were in a typical range for cellulose films (25°). Further SFE (ca 72 mJ/m^2) increased having a rather large polar contribution of ca 30 mJ/m^2. The reason for this effect was the elimination of the nonpolar alkyl chains and TMS groups.

3.6. UV-Vis spectroscopy

Since Bi_2S_3 is known as material with a low band gap, UV-VIS was employed to check the suitability of this material as light absorber in TMSC and cellulose films. For this purpose, the films have been deposited on glass slides instead of silicon wafers. Fig. 8 compares the TMSC/BiXa films before and after thermal treatment. It can be clearly seen that after the heat treatment the initial absorption band of the BiXa at ca. 380 nm vanished while the characteristic spectrum of Bi_2S_3 nanoparticles with an onset between 800 – 900 nm appeared. The TMSC and regenerated cellulose matrix material (for TMSC and TMSC heated see Fig. S7) did not absorb in the Vis region and therefore did not affect the absorption of the Bi_2S_3 nanoparticles.

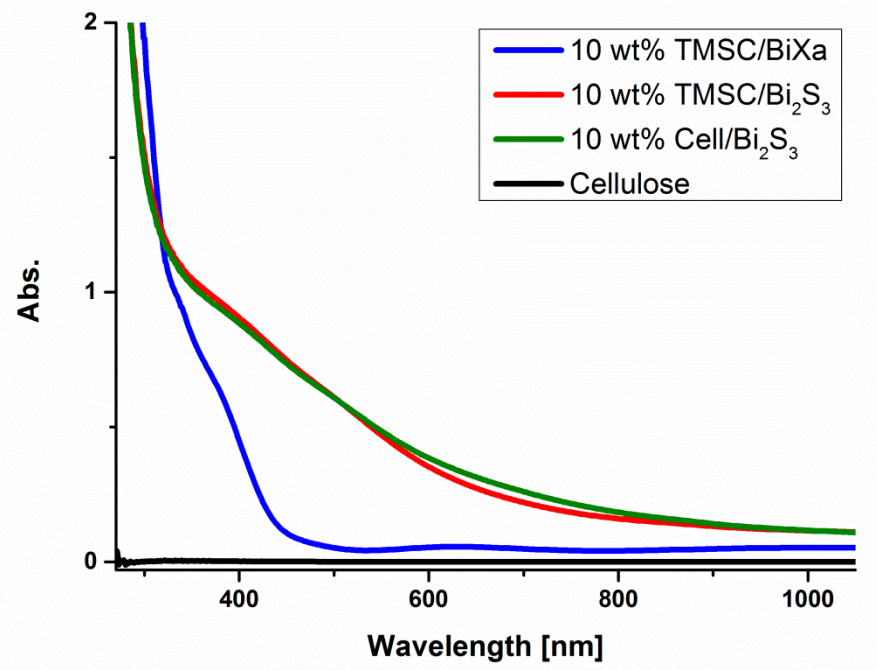

Figure 8. UV-VIS absorption spectra of the 10 wt.% native, heat treated, regenerated and cellulose reference sample.

The determination of the band gap of the nanocomposite films yielded 1.76 eV which is within the range of reported values for bismuth sulfides. Additional data can be found in the Supplementary Materials (Figure S8).

4. Conclusions

In summary, we successfully demonstrated the generation of bismuth sulfide cellulose nanocomposites based on BiXa and TMSC. Spin coating of chloroform solutions containing BiXa and TMSC onto solid substrates yielded for a variety of BiXa:TMSC ratios homogeneous films, whereas the BiXa was successfully converted in all cases to rod-like Bi_2S_3 nanoparticles in a subsequent heating step under exclusion of oxygen and moisture. The conversion of the BiXa to the Bi_2S_3 nanoparticles was further monitored *in-situ* using GI-SWAXS experiments at a synchrotron facility and yielded together with TEM particle with a diameter of 25±4 nm and a

length of 80±7 nm. The morphology of the films depends on the ratio of the initial amount of BiXa in the films and ranged from smooth (1 wt.%) to rough (10 wt.%). After the particles had formed, the silyl groups were cleaved off using HCl vapors under TMSCl elimination to obtain cellulose-Bi_2S_3 nanocomposite films. This procedure affected the roughness as well as the thickness of the films since this conversion was associated with a shrinkage of the film due to the formation of hydrogen bonds (E. Kontturi et al., 2011). Depending on whether the silyl groups were cleaved or not, the wettability of the nanocomposite films was either hydrophobic or hydrophilic. This enables a maximum in flexibility given the case if these films should be embedded into devices. In principle, it is further possible to obtain partially regenerated films (Tamilselvan Mohan et al., 2011) whereas in this case the resulting surface free energies are somewhere in between fully regenerated cellulose and non-regenerated TMSC, opening further the processing window for making devices. Finally, the conversion of the BiXa to the bismuth sulfide particles resulted in a change of color due to the low band gap (1.76 eV) of the nanoparticles which was quantified by UV-Vis spectroscopy. It clearly turned out that the observed absorptions correspond well to already published spectra of Bi_2S_3 nanoparticles. In future studies, we will focus how to use this approach in the generation of cellulose based photovoltaic devices.

5. Acknowledgements

Part of the work was supported by the People Programme (Marie Curie Actions – Career Integration Grants) of the European Union's Seventh Framework Programme (FP7/2007-2013) under REA grant agreement n°618158 (PhotoPattToCell) and the H2020-FET-open project CONQUER under grant agreement n°665172. Elettra Sincrotrone is acknowledged for providing synchrotron radiation at the Austrian SAXS beamline. The authors thank Jürgen Sattelkow and

Sebastian Dunst for technical support. Dr. Thomas Rath is gratefully acknowledged for discussions.

References

Ahmad, M., Rafiq, M. A., Rasool, K., Imran, Z., & Hasan, M. M. (2013). Dielectric and transport properties of bismuth sulfide prepared by solid state reaction method. *Journal of Applied Physics*, 113(4), 043704.

Breitwieser, D., Kriechbaum, M., Ehmann, H. M. A., Monkowius, U., Coseri, S., Sacarescu, L., & Spirk, S. (2015). Photoreductive generation of amorphous bismuth nanoparticles using polysaccharides – Bismuth–cellulose nanocomposites. *Carbohydrate Polymers*, 116, 261-266.

Cooper, G. K., Sandberg, K. R., & Hinck, J. F. (1981). Trimethylsilyl cellulose as precursor to regenerated cellulose fiber. *Journal of Applied Polymer Science*, 26(11), 3827-3836.

Ehmann, H. M. A., Werzer, O., Pachmajer, S., Mohan, T., Amenitsch, H., Resel, R., Kornherr, A., Stana-Kleinschek, K., Kontturi, E., & Spirk, S. (2015). Surface-Sensitive Approach to Interpreting Supramolecular Rearrangements in Cellulose by Synchrotron Grazing Incidence Small-Angle X-ray Scattering. *ACS Macro Letters*, 713-716.

Jung, H., Park, C.-M., & Sohn, H.-J. (2011). Bismuth sulfide and its carbon nanocomposite for rechargeable lithium-ion batteries. *Electrochimica Acta*, 56(5), 2135-2139.

Kaltenhauser, V., Rath, T., Haas, W., Torvisco, A., Muller, S. K., Friedel, B., Kunert, B., Saf, R., Hofer, F., & Trimmel, G. (2013). Bismuth sulphide-polymer nanocomposites from a highly soluble bismuth xanthate precursor. *Journal of Materials Chemistry C*, 1(47), 7825-7832.

Konstantatos, G., Levina, L., Tang, J., & Sargent, E. H. (2008). Sensitive Solution-Processed Bi2S3 Nanocrystalline Photodetectors. *Nano Letters*, 8(11), 4002-4006.

Kontturi, E., & Lankinen, A. (2010). Following the Kinetics of a Chemical Reaction in Ultrathin Supported Polymer Films by Reliable Mass Density Determination with X-ray Reflectivity. *J. Am. Chem. Soc.*, 132(11), 3678-3679.

Kontturi, E., Suchy, M., Penttilä, P., Jean, B., Pirkkalainen, K., Torkkeli, M., & Serimaa, R. (2011). Amoprhous Characteristics of an Ultrathin Cellulose Film. *Biomacromolecules*, 12, 770-777.

Kontturi, E., Thüne, P. C., & Niemantsverdriet, J. W. (2003). Cellulose Model Surfaces Simplified Preparation by Spin Coating and Characterization by X-ray Photoelectron

Spectroscopy, Infrared Spectroscopy, and Atomic Force Microscopy. *Langmuir,* 19(14), 5735-5741.

Li, H., Yang, J., Zhang, J., & Zhou, M. (2012). Facile synthesis of hierarchical Bi2S3 nanostructures for photodetector and gas sensor. *RSC Advances,* 2(15), 6258-6261.

Liu, G.-Y., Xu, L.-Y., Zhou, F., Zhang, Y., Li, H., Xu, Q. F., & Lu, J. M. (2013). Dynamic random access memory devices based on bismuth sulfide nanoplates prepared from a single source precursor. *Physical Chemistry Chemical Physics,* 15(27), 11554-11558.

Martinez, L., Stavrinadis, A., Higuchi, S., Diedenhofen, S. L., Bernechea, M., Tajima, K., & Konstantatos, G. (2013). Hybrid solution-processed bulk heterojunction solar cells based on bismuth sulfide nanocrystals. *Physical Chemistry Chemical Physics,* 15(15), 5482-5487.

Mohan, T., Kargl, R., Doliška, A., Vesel, A., Köstler, S., Ribitsch, V., & Stana-Kleinschek, K. (2011). Wettability and surface composition of partly and fully regenerated cellulose thin films from trimethylsilyl cellulose. *Journal of Colloid and Interface Science,* 358(2), 604-610.

Mohan, T., Ristic, T., Kargl, R., Doliska, A., Köstler, S., Ribitsch, V., Marn, J., Spirk, S., & Stana-Kleinschek, K. (2013). Cationically rendered biopolymer surfaces for high protein affinity support matrices. *Chemical Communications,* 49, 11530-11532.

Mohan, T., Spirk, S., Kargl, R., Doliska, A., Vesel, A., Salzmann, I., Resel, R., Ribitsch, V., & Stana-Kleinschek, K. (2012). Exploring the rearrangement of amorphous cellulose model thin films upon heat treatment. *Soft Matter,* 8, 9807-9815.

Orelma, H., Filpponen, I., Johansson, L.-S., Laine, J., & Rojas, O. J. (2011). Modification of Cellulose Films by Adsorption of CMC and Chitosan for Controlled Attachment of Biomolecules. *Biomacromolecules,* 12(12), 4311-4318.

Pradhan, N., Katz, B., & Efrima, S. (2003). Synthesis of High-Quality Metal Sulfide Nanoparticles from Alkyl Xanthate Single Precursors in Alkylamine Solvents. *Journal of Physical Chemistry B,* 107(50), 13843-13854.

Rabin, O., Manuel Perez, J., Grimm, J., Wojtkiewicz, G., & Weissleder, R. (2006). An X-ray computed tomography imaging agent based on long-circulating bismuth sulphide nanoparticles. *Naturet Materials,* 5(2), 118-122.

Wang, Y. Y., Cai, K. F., & Yao, X. (2012). One-pot fabrication and enhanced thermoelectric properties of poly(3,4-ethylenedioxythiophene)-Bi2S3 nanocomposites. *Journal of Nanoparticle Research*, 14(5), 1-7.

Wang, Z., Qu, S., Zeng, X., Liu, J., Tan, F., Jin, L., & Wang, Z. (2010). Influence of interface modification on the performance of polymer/Bi2S3 nanorods bulk heterojunction solar cells. *Applied Surface Science*, 257(2), 423-428.

Wolfberger, A., Petritz, A., Fian, A., Herka, J., Schmidt, V., Stadlober, B., Kargl, R., Spirk, S., & Griesser, T. (2015). Photolithographic patterning of cellulose: a versatile dual-tone photoresist for advanced applications. *Cellulose*, 22, 717-727.

Yao, K., Gong, W. W., Hu, Y. F., Liang, X. L., Chen, Q., & Peng, L. M. (2008). Individual Bi2S3 Nanowire-Based Room-Temperature H2 Sensor. *Journal of Physical Chemistry C*, 112(23), 8721-8724.

Yao, K., Zhang, Z. Y., Liang, X. L., Chen, Q., Peng, L. M., & Yu, Y. (2006). Effect of H2 on the Electrical Transport Properties of Single Bi2S3 Nanowires. *Journal of Physical Chemistry B*, 110(43), 21408-21411.